Fabrication of kW-level chirped and tilted fiber Bragg gratings and filtering of stimulated Raman scattering in high-power CW oscillators

Kerong Jiao[1], Jian Shu[2], Hua Shen[1,2], Zhiwen Guan[1], Feiyan Yang[1], and Rihong Zhu[1,2]

[1]*MIIT Key Laboratory of Advanced Solid Laser, Nanjing University of Science and Technology, Nanjing 210094, China*

[2]*School of Electronic Engineering and Optoelectronic Technology, Nanjing University of Science and Technology, Nanjing 210094, China*

Abstract

Suppression of stimulated Raman scattering (SRS) by means of chirped and tilted fiber Bragg gratings (CTFBGs) has become a key topic. However, research on high-power systems is still lacking due to two problems. Firstly, after the inscription, there are a large number of hydroxyl compounds and hydrogen molecules in CTFBGs that cause significant heating due to their strong infrared absorption. Secondly, CTFBGs can couple Stokes light from the core to the cladding and the coating, which causes serious heating in the coating of the CTFBG. Aimed at overcoming these bottlenecks, a process that combines constant-low-temperature and variable-high-temperature annealing is used to reduce the thermal slope of the CTFBG. Also, a segmented-corrosion cladding power stripping technology is used on the CTFBG to remove the Stokes light which is coupled to the cladding, which solves the problem of overheating in the coating of the CTFBG. Thereby, a CTFBG with both a kilowatt-level power-carrying load and the ability to suppress SRS in a fiber laser has been developed. Further, we establish a kW-level CW oscillator to test the CTFBG. Experimental results demonstrate that the power-carrying load of the CTFBG is close to 1 kW, the thermal slope is lower than 0.015 °C/W, and the SRS suppression ratio is nearly 23 dB.

Keywords: chirped and tilted fiber Bragg gratings; fiber optics components; high-power fiber laser; stimulated Raman scattering

1. Introduction

Fiber lasers have been widely used in many fields, including industrial processing[1, 2], biomedicine[3, 4] and communication[5], due to their compact structure, high efficiency and high spatial beam quality[6]. With increasing demand for high power, stimulated Raman scattering (SRS) has become one of the main factors limiting the development of fiber lasers[7]. To solve this problem in recent years, an increasing number of researchers have focused their attention on using specially structured fiber gratings to suppress the SRS in fiber lasers.

One such method is to use long-period fiber gratings (LPGs). LPGs, usually used in the sensing field[8, 9], can couple the forward-propagating core modes to the forward-propagating cladding modes. Therefore, a specific wavelength of light can be coupled from the core to the cladding by controlling the period of the LPG. In 2010, Nodop

et al.[10, 11] used this characteristic of LPGs to suppress SRS in pulsed fiber lasers with an average power of 70 µW and a suppression ratio exceeding 20 dB (99%). However, LPGs are sensitive to temperature, strain and bending, which leads to a drift in the cladding-mode resonances and a reduction of the suppression ratio. Another approach is to use CTFBGs. Unlike LPGs, CTFBGs can couple the forward-propagating core modes to the backward-propagating cladding modes. Furthermore, compared with LPGs, the period of a CTFBG is much smaller, which means the cladding-mode resonances of CTFBGs change only slightly under the influence of temperature, strain and bending. This makes CTFBGs the preferred method of suppressing SRS by fiber gratings. In 2014, Liu *et al.*[12] introduced chirp into a TFBG and realized the design and inscription of a CTFBG with broadband filtering for the first time. Moreover, potential applications of CTFBGs in the field of sensing and communication were also proposed. Wang *et al.*[13] first applied a CTFBG to a 22 W low-power CW fiber laser to suppress the SRS in 2017, and reported a 25 dB (99.68%) SRS suppression ratio. Further, they achieved inscription of a CTFBG in PS-GDF-

Correspondence to: H. Shen, MIIT Key Laboratory of Advanced Solid Laser, Nanjing University of Science and Technology, Nanjing 210094, China. Email: edward_bayun@163.com

20/400 photosensitive fiber in 2018[14], and applied it in the seed of a master oscillator power amplifier (MOPA) structure fiber laser with a 4.2 kW output power in 2019 to suppress the SRS in a 100 W-level seed[15]. However, they did not consider the power-carrying load of the CTFBG in the case of high power. The reason is that fiber gratings made of photosensitive fibers are usually used in the field of low-power lasers, such as sensing and communication[16, 17]. Compared with the large-mode-area passive fiber gratings used in high-power fiber lasers, their power-carrying load is worse. In short, CTFBGs which can suppress SRS are still at low power and research on CTFBGs with kW-level power-carrying loads is still lacking.

High-power fiber gratings usually use LMA-GDF-20/400 double-cladding passive fiber and can carry thousands of watts of signal light. Therefore, CTFBGs made of LMA-GDF-20/400 fiber are one of the most promising passive devices for SRS suppression in kW-level CW high-power fiber lasers. However, no research has been carried out in this area – mainly for two reasons. Firstly, LMA-GDF-20/400 passive fiber is only weakly photosensitive, so to realize the inscription of a high-reflectivity grating, the fiber should be previously processed by hydrogenation. However, a large number of hydroxyl compounds are generated in the CTFBGs after the inscription, while there are still a large number of unreacted hydrogen molecules in the CTFBG. These materials cause significant heating in the high-power case due to strong infrared absorption, which greatly limits the power-carrying load of CTFBGs. Secondly, CTFBGs can couple Stokes light from the core to the cladding and coating, which will cause serious heating in the coating of the CTFBG in the incident direction of the laser at high power.

Aimed at overcoming these technical bottlenecks, a process that combines constant-low-temperature and variable-high-temperature annealing is used to reduce the thermal slope of the CTFBG. In addition, a segmented-corrosion cladding power stripping technology is used on a CTFBG for the first time to remove the Stokes light coupled to the cladding by the CTFBG, which solves the problem of overheating in the coating of the CTFBG in the incident direction of the laser. Thereby, a CTFBG with both a kilowatt-level power-carrying load and the ability to suppress SRS in a fiber laser has been developed. Further, a kW-level CW oscillator system is established to test the power-carrying load of the CTFBG and its SRS suppression ratio. To the best of our knowledge, this is the first time that a CTFBG has been applied to a kW-level fiber laser system to suppress the SRS.

2. Design and simulation of high-power CTFBG

As shown in Figure 1(a), the difference between a CTFBG and a chirped fiber Bragg grating (CFBG) is that there is an angle between the fiber axis and the grating plane, so that the
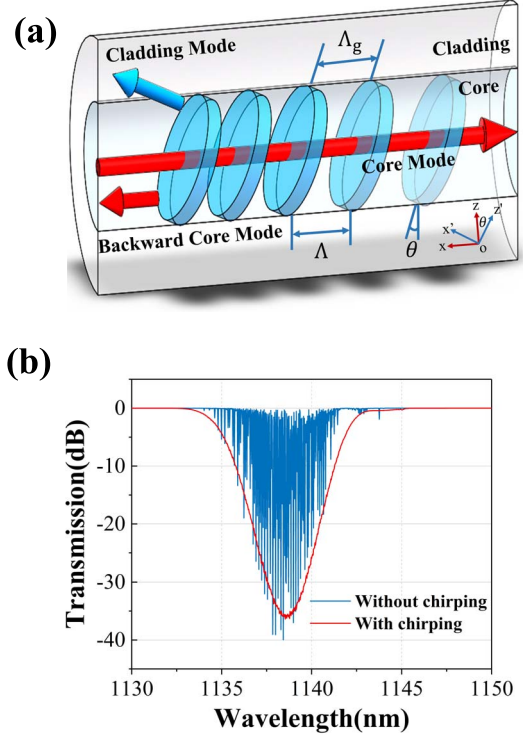

Figure 1. (a) Schematic diagram of the structure of a CTFBG and (b) simulated transmission spectra of a TFBG and a CTFBG with a tilt angle of 4°; the chirp rate of the CTFBG is 0.3 nm/cm.

forward core modes, which were originally transmitted only in the core, are coupled to the backward core modes and the cladding modes.

The spectrum of a TFBG will not only have one core-mode resonance, but also many cladding-mode resonances[8], as shown by the solid blue line in Figure 1(b). The direction along the fiber is designated as the x-axis and the direction perpendicular to the grid plane is the x'-axis. Due to the tilted grating plane, the period of the grating along the x'-direction is Λ_g and the period of the grating along the x-direction is Λ. The relationship between the periods can be expressed as

$$\Lambda = \frac{\Lambda_g}{\cos\theta}, \qquad (1)$$

where θ is the tilt angle between the x-axis and the x'-axis. Similar to a fiber Bragg grating (FBG), the Bragg resonance wavelength for the TFBG can be expressed as

$$\lambda_B = \frac{2n_{\text{core}}\Lambda_g}{\cos\theta}, \qquad (2)$$

where n_{core} is the effective refractive index of the core mode. The cladding-mode resonance wavelength can be expressed as

$$\lambda_{\text{clad},i} = \frac{(n_{\text{clad},i} + n_{\text{core})\Lambda_g}}{\cos\theta}, \qquad (3)$$

where $n_{\text{clad},i}$ is the effective refractive index of the ith cladding mode. When chirp is introduced into a TFBG, multiple resonances will overlap to form a widened resonance band[12], as shown by the solid red line in Figure 1(b). Then Λ_g can be expressed as

$$\Lambda_g(z) = \Lambda_0 + \frac{C}{2n_{\text{core}}}z \quad \left(-\frac{L}{2} \leqslant z \leqslant \frac{L}{2}\right), \quad (4)$$

where Λ_0 is the period in the middle of the grating, C is the chirp constant and L is the length of the grating. The wavelengths of the core mode and the ith cladding mode of the CTFBG can be expressed as

$$\lambda_B(z) = \frac{2n_{\text{core}}\Lambda_g(z)}{\cos\theta}, \quad (5)$$

$$\lambda_{\text{clad},i}(z) = \frac{(n_{\text{clad},i} + n_{\text{core}})\Lambda_g(z)}{\cos\theta}. \quad (6)$$

The bandwidth of the ith cladding mode may be expressed as

$$\Delta\lambda_{\text{clad},i} = \frac{(n_{\text{core}} + n_{\text{clad},i})(\Lambda_{g(\max)} - \Lambda_{g(\min)})}{\cos\theta}, \quad (7)$$

where $\Lambda_{g(\max)}$ and $\Lambda_{g(\min)}$ are the longest and shortest periods of the grating, respectively.

The output spectrum of a 1080 nm fiber laser was simulated, as shown in Figure 2(a). The central SRS wavelength is about 1138 nm and the 20 dB bandwidth is 20 nm. In order to suppress the SRS, we simulated the CTFBGs with different parameters in the LMA-GDF-20/400 double-cladding fiber (Nufern Inc.). The period of the phase mask is 394.5 nm and the grating length is 40 mm. Figure 2(b) shows the simulation of transmission spectra of CTFBGs with different tilt angles – the chirp rate is 1.5 nm/cm and the index modulation amplitude is 0.001. According to the simulation results, an excessive tilt angle will cause the wavelength of the cladding resonance to move towards shorter wavelengths, with a concomitant reduction in reflectivity. Figure 2(c) is the simulation of transmission spectra of CTFBGs with different chirp rates – the tilt angle is 4° and the index modulation amplitude is 0.001. From Figure 2(c), we can see that the bandwidth of the CTFBG increases with an increase in the chirp rate; however, the reflectivity of the CTFBG decreases. Therefore, in order to balance the tilt angle, resonance wavelength and reflectivity, we selected 4° as the tilt angle and 1.5 nm/cm as the chirp rate of our CTFBG. At this angle and chirp rate, the reflectivity of the CTFBG can exceed 20 dB (99%), while the wavelength range of the Stokes light stimulated by the 1080 nm laser is completely spanned.

3. Inscription of high-power CTFBGs

Figure 3(a) shows the inscription system. An argon ion laser (Innova 90C FreD Ion Laser, Coherent Inc.) produces CW
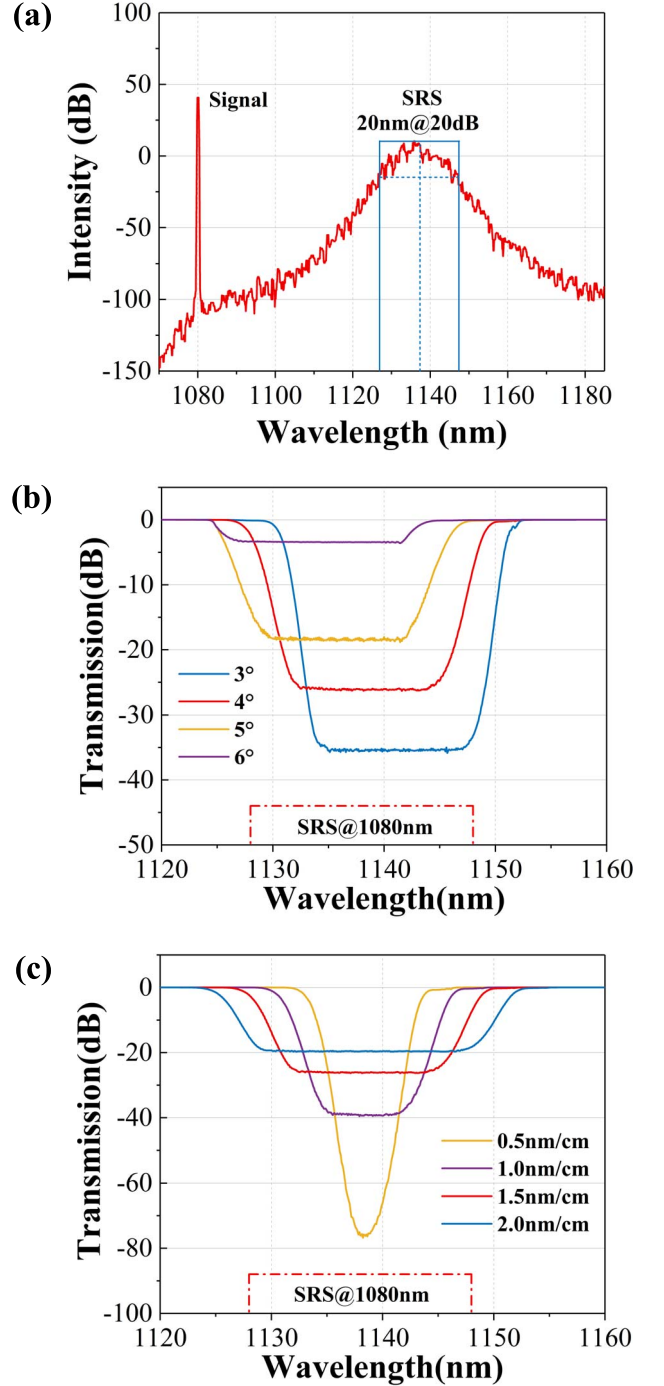
Figure 2. Simulation of (a) the SRS spectrum of 1080 nm fiber laser, (b) transmission spectra of CTFBGs with different tilt angles and (c) transmission spectra of CTFBGs with different chirp rates.

ultraviolet laser with a wavelength of 244 nm and an output power of 100 mW. A UV reflector is used to reflect the laser to the cylindrical lens ($f = 250\,\text{mm}$), and the laser spot is compressed longitudinally through the cylindrical lens to improve the power density at the fiber core. A stepping motor moves along the horizontal direction at uniform speed
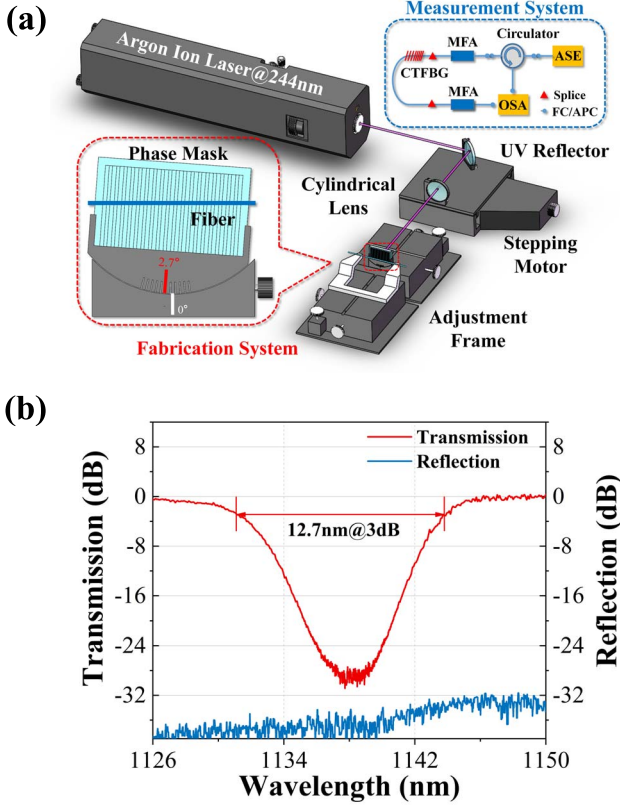
Figure 3. (a) Inscription system based on a tilted-phase-mask method with an online parameter measurement system and (b) the resulting CTFBG spectral measurement.

(0.0013 mm/s) to achieve the inscription of the CTFBG. The phase mask (period, 394.5 nm; chirp rate, 1.5 nm/cm; length, 40 mm) and fiber (LMA-GDF-20/400-M, Nufern Inc., which had been previously processed by high-pressure (13 MPa) low-temperature (40 °C) hydrogenation for 32 days) are immobilized on the six-dimensional adjustment frame. The distance between the fiber and the phase mask is controlled to be about 20 μm.

During the inscription, the tilt angle was controlled by rotating the phase mask. According to the literature[18], the actual tilt angle of the grating plane is calculated by

$$\theta_R = \pi/2 - \arctan(n_{uv} \tan\theta)^{-1}, \qquad (8)$$

where n_{uv} is the refractive index of the fiber core at 244 nm, which we approximate here as 1.452. Thus, in order to realize the inscription of the CTFBG with a 4° tilt angle, the phase mask, relative to the fiber, was rotated to 2.7°. As Figure 3(a) shows, the light emitted by the amplified spontaneous emission (ASE) source (VASS-1060-B-13-GF, Connect Fiber Optics Corporation) is coupled into the CTFBG through the circulator and mode field adapter (MFA), and then coupled into the optical spectrum analyzer (OSA; AQ6730D, Yokogawa Corporation) by another MFA

so as to monitor spectral information, such as the reflectivity, central wavelength and bandwidth, of the CTFBG in real time. Figure 3(b) shows the spectrum of the CTFBG after inscription; the solid red line is the transmission spectrum, from which we can see that the reflectivity of the CTFBG is higher than 28 dB (99.8%) and the full-width at half-maximum (FWHM) is 12.7 nm, and the solid blue line is the reflectance spectrum of the CTFBG. The backward-propagating cladding modes cannot be observed in the reflectance spectrum because the energy carried by these modes is lost due to bending of the fiber. There are only some weak 'ghost' modes in the reflectance spectrum, which are composed of low-order cladding modes[12].

4. Heat treatment of high-power CTFBGs

The suppression of SRS using CTFBGs has achieved good results in low-power fiber lasers, but research into this method is still lacking at high power due to significant heating of the CTFBG.

There are two reasons for the heating of the CTFBG. The first is that photo-induced reactions in the hydrogenated fiber can easily produce significant amounts of Ge–OH and Si–OH bonds in the CTFBG during the writing process[19]. Moreover, there remains a large number of unreacted hydrogen molecules in fiber after inscription. When high-power radiation propagates in the grating, these materials will cause significant heating due to the strong infrared absorption characteristics, which limits the power that may be carried by the CTFBG. Figure 4(a) shows a thermal image of our inscribed CTFBG without annealing (acquired by a Fluke Ti400 Infrared Imager). When the signal power was raised to 100 W, the grating temperature reached 60 °C and the thermal slope was 0.37 °C/W (room temperature, 23 °C).

Hence, we have adopted two different annealing methods for dissociative hydrogen molecules and hydroxyl to improve the power-carrying load of the CTFBG. First, the CTFBG is annealed under constant low temperature. The grating is held at 60 °C for 30 days to remove residual dissociative hydrogen molecules. Then, the grating is annealed at various high temperatures. As shown in Figure 4(b), the grating is slowly heated to 300 °C in intervals of 50 °C, from room temperature, and remains at 300 °C for 15 min, before being gradually reduced to room temperature. The purpose of annealing at high temperature is to reduce the hydroxyl concentration in the grating, which we believe proceeds via the reaction[20]

$$2(Si(Ge)\text{–}OH) \xrightarrow{\text{Heat}} Si(Ge)\text{–}O\text{–}Si(Ge) + H_2O. \quad (9)$$
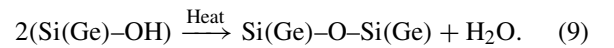
High temperature causes the hydroxyl to break up and form water molecules, which accelerates thermal diffusion of water molecules away from the grating. The purpose of stepped heating and cooling is to avoid residual thermal
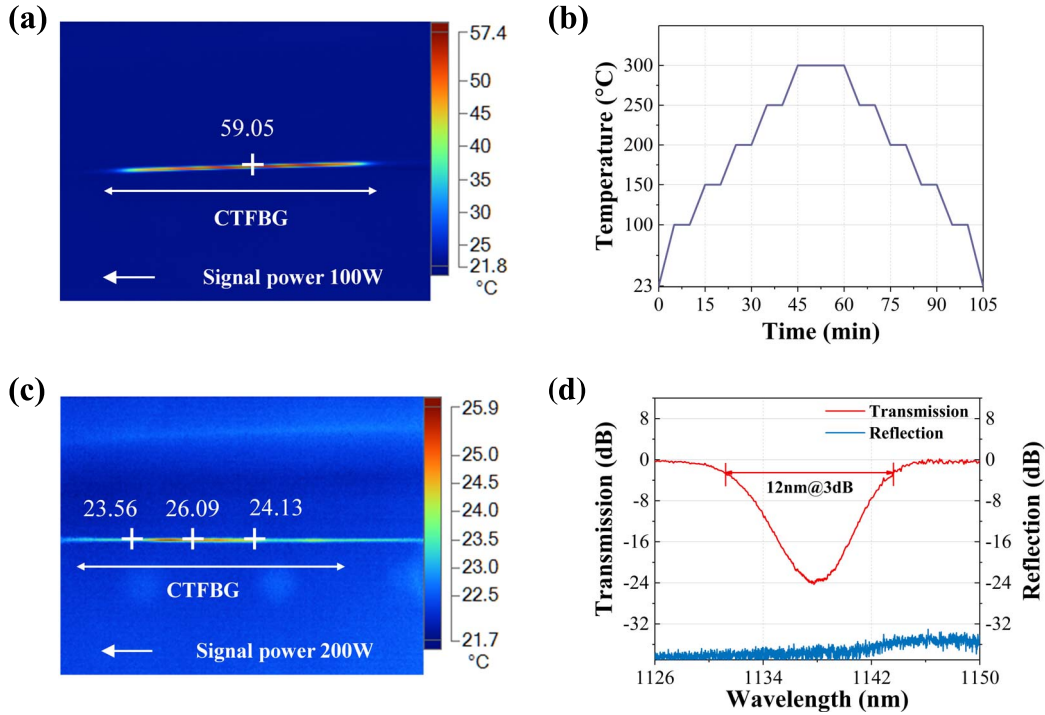
Figure 4. (a) Thermal image of the CTFBG without annealing; (b) schematic diagram of the temperature variation in the high-temperature annealing; (c) thermal image of the CTFBG after annealing; (d) spectrum of the CTFBG after annealing.

stress inside the grating caused by a drastic change of temperature. Figure 4(c) shows the thermal image of the CTFBG after annealing. When the signal power is raised to 200 W, the grating temperature is 26 °C and the thermal slope is 0.015 °C/W, which is 96% lower than that measured before annealing. In Figure 4(d) the spectrum of CTFBG after annealing shows that the reflectivity of the CTFBG is 24 dB (99.6%), which is 0.2% lower than that measured before annealing, and the FWHM is narrowed to 12 nm.

Another reason for the heating of the CTFBG is that it couples the forward-propagating core modes to the backward-propagating cladding modes, and the cladding radiation satisfies the total reflection condition at the air–cladding interface and continues to transmit backwards. The refractive index of the coating is higher than that of the air, and because the cladding radiation does not satisfy the total reflection condition when transmitted through the coating–cladding interface, the cladding radiation enters the coating and is absorbed by it. As a result, heat is generated, as Figure 5(a) shows. This heating phenomenon intensifies with increasing power, and can even cause burning up of the CTFBG. As shown in Figure 5(b), the coating temperature exceeded 40 °C when the signal power was 100 W (room temperature, 23 °C).

To solve this problem, a method that combines the CTFBG with cladding light stripping technology is proposed for the first time. The segmented-corrosion method[21, 22] proposed by our group is used to etch the grating surface of the

CTFBG, so as to strip the Stokes light coupled to the cladding. The structure of the stripper is shown in Figure 5(c). Hydrofluoric acid is used to etch the surface of the fiber cladding, in which the corrosion section is divided into two sections, and the surface roughness increases gradually from the first segment to the last segment (the roughness of L_2 is greater than that of L_1, the length of L_1 is about 4 mm and the length of L_2 is about 7 mm). Compared with the single-segment corrosion method, this method can effectively improve stripping uniformity and avoid the problem of local overheating caused by single-section corrosion. Furthermore, the power-carrying load of the stripper has been greatly improved. The temperature of the coating after constructing the stripper is shown in Figure 5(d). When the signal power reaches 982 W (the power-carrying load at the CTFBG is 982 W), the coating temperature is 28.6 °C and the temperature of the CTFBG is 36.5 °C (the thermal slope is lower than 0.015 °C/W).

5. SRS suppression effect of high-power CTFBG

Finally, we tested the SRS suppression ratio of the CTFBG. The high-power testing system is shown in Figure 6, for which we adopted a bidirectional pump structure (the pump power is 1500 W) and a 915 nm pump source to realize a 1080 nm laser output (the output power is 982 W). The linear laser cavity consists of a pair of fiber Bragg gratings (FBGs) whose central reflective wavelengths are 1080 nm
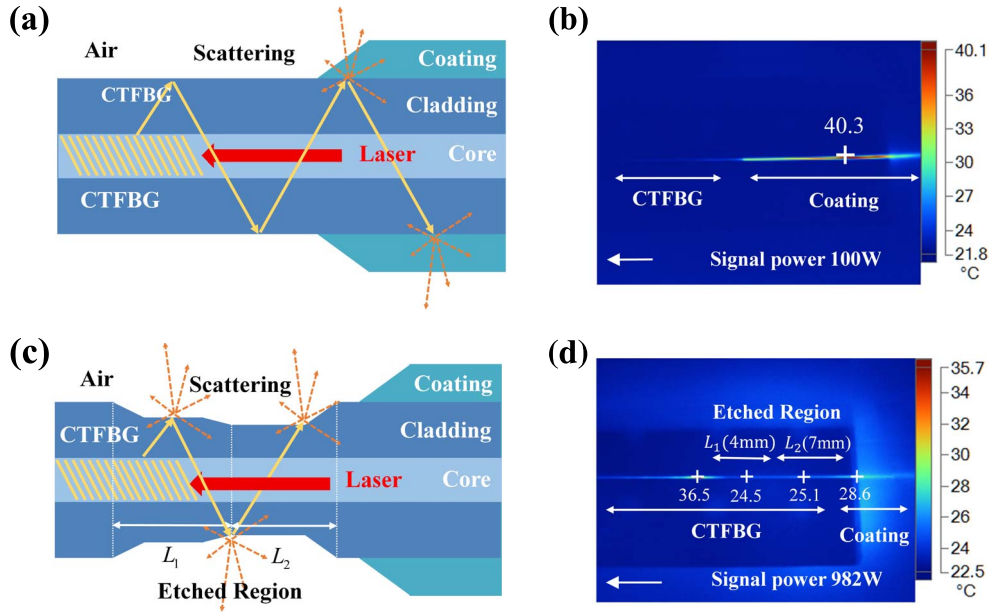
Figure 5. (a) Schematic diagram of the heating of the coating in the laser incident direction and (b) thermal image of the CTFBG without a stripper. (c) Schematic diagram of the stripper constructed by the method of segmented corrosion and (d) thermal image of the CTFBG with a stripper.
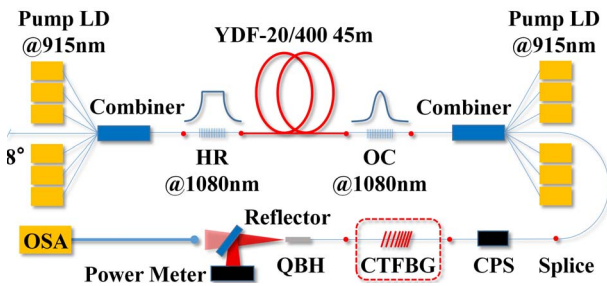

Figure 6. kW-level high-power testing system.

and a gain fiber with a core/cladding diameter of 20/400 μm (LAM-YDF-20/400-M, Nufern Inc.). The reflectivity of the highly reflective (HR) FBG is greater than 99.9% and that of the output coupling (OC) FBG is 10%. The length of the gain fiber used in the system is about 45 m. The CTFBG is inserted between the cladding power stripper (CPS) and a quartz block of high power (QBH), and the temperature of the CTFBG is monitored in real time by an infrared thermal imager. The output laser is reflected by an infrared reflector (reflectivity >99.8%) and then incident on the power meter. The laser transmitted by the reflector is spectroscopically measured to test the SRS suppression ratio of the CTFBG (the position of the detector is fixed before and after inserting the CTFBG into the system).

Before testing the SRS suppression ratio of the CTFBG, we measured the insertion loss of the CTFBG and obtained approximately 0.143 dB (3.25%). Then we tested the SRS suppression ratio of the CTFBG. Figure 7(a) shows the output spectrum of the testing system when the CTFBG is

not inserted. When the laser output power reached 982 W (pump power is 1500 W), the SRS power was calculated to be roughly 47 W, according to the difference between the peaks of the signal light and SRS in the spectrum; this is equivalent to about 13 dB (that is, the power of SRS is 5% of the signal power). Figure 7(b) shows the output spectrum of the testing system with the CTFBG. When the laser output power is 906 W (pump power is 1500 W), the SRS spectral signal is almost invisible. The yellow solid line in Figure 7(c) is the difference between the output spectra of the system measured with and without the CTFBG, at 1500 W pump power, which represents the SRS suppression ratio of the CTFBG; the curve is fitted to remove the effects of noise (solid blue line in Figure 7(c)) and the SRS suppression ratio of the CTFBG is close to 23 dB (99.5%).

6. Conclusion

Aimed at providing a high-power CTFBG, a process that combines constant-low-temperature and variable-high-temperature annealing is used to reduce the thermal slope of the CTFBG. In addition, segmented-corrosion cladding power stripping technology is used on the CTFBG for the first time to remove the Stokes light coupled to the cladding by the CTFBG, which solves problem of overheating in the coating of the CTFBG in the incident direction of the laser. Thereby, a CTFBG with both a kilowatt-level power-carrying load and the ability to suppress SRS in a fiber laser has been developed. Furthermore, the power-carrying load and the thermal slope of the CTFBG were tested by means of
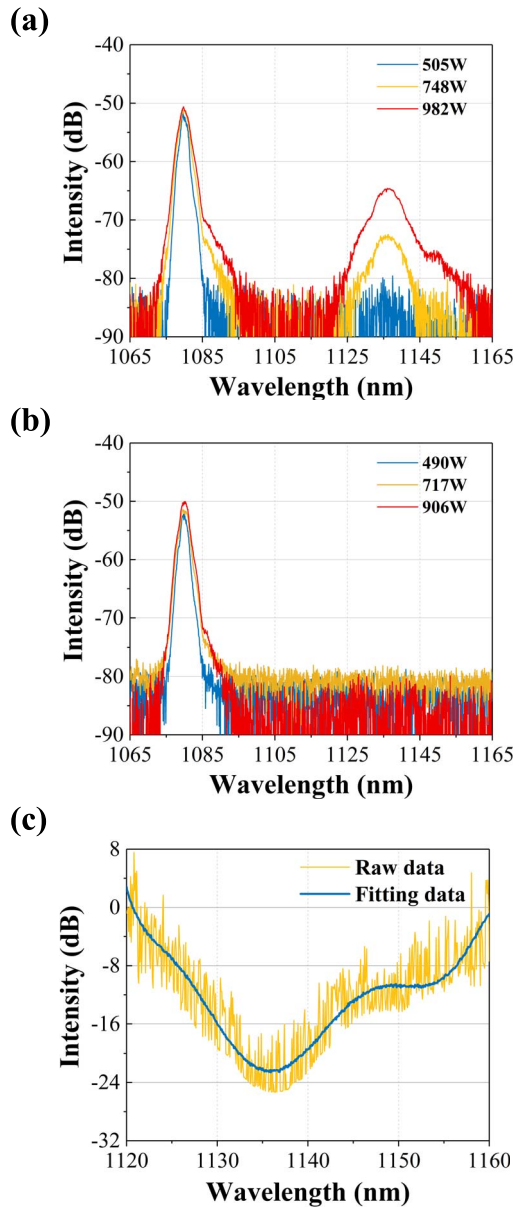
(a)

(b)

(c)

Figure 7. Output spectra of the testing system (a) without the CTFBG and (b) with the CTFBG; (c) the difference between the output spectra of the system with and without the CTFBG.

a high-power CW oscillator. The results show that the power-carrying load of the CTFBG is near to 1 kW and the thermal slope is less than 0.015 °C/W. Moreover, suppression of SRS in a kW-level CW fiber laser was realized by a CTFBG for the first time, with a suppression ratio close to 23 dB. The results of this paper should promote further development

of high-power CTFBG technology with SRS suppression functionality, so that CTFBGs in the future can be widely used in high-power fiber lasers to control the output spectra.

Acknowledgements

References

1. L. Quintino, A. Costa, R. Miranda, D. Yapp, V. Kumar, and C. J. Kong, Mater. Des. **28**, 1231 (2007).
2. L. D. Scintilla and L. Tricarico, Opt. Eng. **52**, 076115 (2013).
3. N. M. Fried and K. E. Murray, J. Endourol. **19**, 25 (2005).
4. K. D. Polder and S. Bruce, Dermatol. Surg. **38**, 199 (2012).
5. Z. Li, A. M. Heidt, N. Simakov, Y. Jung, J. M. O. Daniel, S. U. Alam, and D. J. Richardson, Opt. Express **21**, 26450 (2013).
6. Y. B. Wang, G. Chen, and J. Y. Li, High Power Laser Sci. Eng. **6**, e40 (2018).
7. H. W. Zhang, P. Zhou, H. Xiao, J. Y. Leng, R. M. Tao, X. L. Wang, J. M. Xu, X. J. Xu, and Z. J. Liu, High Power Laser Sci. Eng. **6**, e51 (2018).
8. M. Deng, J. S. Xu, Z. Zhang, Z. Y. Bai, S. Liu, Y. Wang, Y. Zhang, C. R. Liao, W. Jin, G. D. Peng, and Y. P. Wang, Opt. Express **25**, 14308 (2017).
9. Z. L. Li, S. Liu, Z. Y. Bai, C. L. Fu, Y. Zhang, Z. Y. Sun, X. Y. Liu, and Y. P. Wang, Opt. Express **26**, 24114 (2018).
10. F. Jasen, D. Nodop, C. Jauregui, J. Limpert, and A. Tünnerman, Opt. Express **17**, 16255 (2009).
11. D. Nodop, C. Jauregui, F. Jasen, J. Limpert, and A. Tünnerman, Opt. Lett. **35**, 2982 (2010).
12. F. Liu, T. Guo, C. Wu, B. O. Guan, C. Lu, H. Y. Tam, and J. Albert, Opt. Express **22**, 24430 (2014).
13. M. Wang, Y. J. Zhang, Z. F. Wang, J. J. Sun, J. Q. Cao, J. Y. Leng, X. J. Gu, and X. J. Xu, Opt. Express **23**, 1529 (2017).
14. M. Wang, Z. X. Li, L. Liu, Z. F. Wang, X. J. Gu, and X. J. Xu, Appl. Opt. **57**, 4376 (2018).
15. M. Wang, Z. F. Wang, L. Liu, Q. Hu, H. Xiao, and X. J. Xu, Photon. Res. **7**, 167 (2019).
16. H. Bartelt, S. Grimm, V. Hagemann, M. Rothhardt, W. Ecke, and R. Willsch, Proc. SPIE **4900**, 424 (2002).
17. A. Jantzen, R. H. S. Bannerman, S. A. Berry, J. C. Gates, P. C. Gow, L. J. Boyd, P. G. R. Smith, and C. Holmes, Opt. Lett. **42**, 3741 (2017).
18. S. J. Mihailov, R. B. Walker, P. Lu, H. Ding, X. Dai, C. Smelser, and L. Chen, IEE Proc. Optoelectron. **149**, 211 (2002).
19. L. B. Fu, G. Tan, W. J. Xu, H. L. An, X. M. Cui, X. Z. Lin, and H. D. Liu, Opt. Lett. **25**, 527 (2000).
20. B. W. Zhang and M. Kahrizi, IEEE Sensors J. **7**, 586 (2007).
21. L. Yin, M. J. Yan, Z. G. Han, H. L. Wang, H. Shen, and R. H. Zhu, Opt. Express **25**, 8760 (2017).
22. M. J. Yan, Z. Wang, L. Q. Meng, L. Yin, Z. G. Han, H. Shen, H. L. Wang, and R. H. Zhu, Appl. Opt. **57**, 485 (2018).